Jestr

Journal of Engineering Science and Technology Review 9 (4) (2016) 17- 25

Research Article

JOURNAL OF
Engineering Science and Technology Review

www.jestr.org

Prediction for Tire-Pavement Contact Stress under Steady-State Conditions based on 3D Finite Element Method

Wang Yang [1,*], Sun Tiecheng [2], Lu Yongjie [1] and Si Chundi [1]

[1] *Key Laboratory of Traffic Safety and Control in Hebei, Shijiazhuang Tiedao University, Shijiazhuang 050043, China*
[2] *College of Engineering, University of Alaska Anchorage, Anchorage, AK 99508, United States*

Received 1 June 2016; Accepted 30 July 2016

Abstract

Tire force is one of the important factors influencing mechanical response of pavement structure. Tire force cannot be measured yet under a high-speed rolling condition because of complicated spatial distribution. To provide a representative form of the tire force to pavement mechanical analysis, this paper established an interaction model of rolling tire and rigid surface. To compare with the equivalent single-wheel load for pavement design, an 11.00R20 tire was chosen as a prototype. Steady-state transport analysis was conducted using a mixed Eulerian /Lagrangian approach, in which a rigid body rotation is described in the Eulerian manner and deformation is described in the Lagrangian manner. The influencing mechanism of tire operation parameters on tire force was explored by analyzing the simulation results of tire contact stress under several working conditions. Results demonstrated that three directions of contact stresses, namely, the vertical, longitudinal, and transversal stresses, exist simultaneously under the steady-state rolling condition. Amplitudes of longitudinal and transversal stresses are at the same magnitude with vertical stress, which should not be neglected during the mechanical response analysis of the pavement structure. Tire rolling state, axle load, tire pressure, and pavement friction coefficient could significantly influence the spatial distribution of contact stress, while speed is insignificant to contact stress. The results provide a reference for the establishment of tire force in pavement model, which is the basis of mechanical behaviours and early failure mechanism for pavement surface.

Keywords: Tire-pavement contact stress, Finite element model, Steady-state condition

1. Introduction

Mechanical response of pavement structure is one of the basic problems in pavement engineering field and is the core of disclosing pavement disease mechanism and designing pavement structure. Tire load is the key influencing factor of pavement mechanical behaviors. Spatial distribution pattern of tire load is a popular research topic in pavement, vehicle, and tire engineering.

Equivalent single-wheel load (ESWL) has long been chosen as a pavement design load. It assumes that the tire axle load is 25 kN, the tire footprint is a circle with 21.30 cm diameter, and the contact pressure is recommended as 0.70 MPa vertical uniform load. Therefore, tire force is widely simplified into a circular, uniform, and distributed vertical load in the traditional mechanical response analysis of pavement structure [1], [2], [3], [4]. However, real tire force is a three-way, non-uniform distributed load. Horizontal tire force significantly affects the mechanical response of the pavement surface [5]. Therefore, exploring the distribution characteristics of tire force is important in examining the mechanical behaviors of pavement structure. Tire force is directly influenced by tire structure and service conditions. Thus, analyzing the contact stresses of representative tires under common operating conditions is necessary as it can provide reference for applying three-way tire forces in the pavement model.

* E-mail address: jtxwy@163.com

2. State of the art

Establishing a tire-pavement coupling model enables the application of three-way tire forces to the pavement through the tire. An earlier research on the modeling of a tire-pavement coupling system was conducted by Wang et al., who built a model and validated it with measured contact stresses from an actual radial truck tire [6]. Moslem et al. [7] built a tire-soil coupling model that realistically predicted laboratory test outputs of the modeled tire on soft soil. In these studies, tires were kept static rather than rolling, and they could only apply static three-way tire forces onto the pavement. Xia et al. [8], [9] and Li et al. [10], [11] established a coupling model between low-speed rolling tire and soil and simulated the quasi-static process of the tire-soil coupling system through this model. In the tire-pavement coupling model established by Wang et al. [12], arbitrary linear or angular velocity could be applied onto the tire. This model could be used to simulate the transient process of the tire-pavement coupling system. Although this type of model could realize complicated tire force actions on pavement, it is disadvantageous in relatively complex modeling processes, abundant model nodes, and high-computational expenses.

The classical mechanical study of pavements does not involve tire mechanical behavior analysis. Therefore, to save computation cost, some studies only established the pavement model and replaced the tire model by applying three-way tire forces directly onto a pavement [13], [14], [15], [16]. Measurement and prediction of tire force are the basis of this model type as tire force loading on a pavement must take real tire force as reference.

Field measurement of tire contact stress began in 1959 [17]. At present, various types of sensors have been developed for tire force measurement [18], [19], [20], [21]. De Beer et al. [5], Hernandez et al. [22], and Luo et al. [23] measured tire force by different types of measurement systems. The results confirmed the spatial distribution complexity of tire contact stress. However, only contact stress of low-speed rolling tire could be measured at present, while contact stress of fast rolling tires could not be measured because of technical limitations.

Finite element method provides a new effective means for tire contact stress prediction. It can accurately predict the contact stress of tires rolling steadily under any speed by establishing a coupling model between rolling tire and rigid surface. Yang et al. [24], Wang et al. [25], and Hernandez et al. [26] established models for specific tires and analyzed tire contact stress under various rolling conditions, such as free rolling, braking/acceleration, and cornering.

The remainder of this paper is organized as follows. Section 3 analyzes the steady-state rolling problem of tires based on finite element method, which is adopted to establish a 3D finite element tire. Section 4 predicts the tire contact stress under different working conditions and analyzes the influences of different tire operation parameters on contact stress. Section 5 gives the conclusion.

3. Methodology

3.1 Finite element presentation of a steady-state rolling tire problem

(1) Kinematic equation

A straight-line motion of a tire is shown in Fig. 1. A steady-state tire rolling involves three states: braking, acceleration, and free rolling. The mixed Eulerian/Lagrangian method was applied to establish the steady-state rolling tire model. Rolling problem kinematics was described in terms of a coordinate frame that moves along with ground motion. In this moving frame, rigid-body rotation was described by the Eulerian manner, while material deformation was described by the Lagrangian method.

Suppose the rim center X_0 is the origin, and T axis is the central axis of rigid-body rotation of the tire. T axis passes through X_0. If the tire translation is neglected and the pavement is simplified into a rigid surface that moves at linear velocity v_0, the tire-rolling problem is converted into a problem in which the tire rotates around the fixed axis at an angular velocity ω and the tire comes in contact with the moving-rigid surface.

As the tire is a flexible body, motions at different points can be decomposed into two parts (Fig. 2). For any point X, it conducts rigid rolling and arrives at point Y accompanied with an infinitesimal displacement to point y. The relationship between points X and Y can be described as

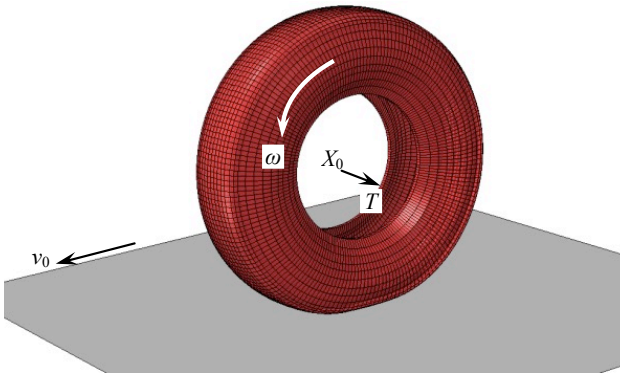

Fig. 1. Description of a rigid-tire rotation

$$\begin{cases} Y = R_S \cdot X \\ R_S = \exp\left(\hat{\omega} t\right) \end{cases} \tag{1}$$

where R_S is the spinning-rotation matrix, $\hat{\omega}$ is the skewed-symmetric matrix related to the rotation vector $\omega = \omega \mathrm{T}$, and t is time.

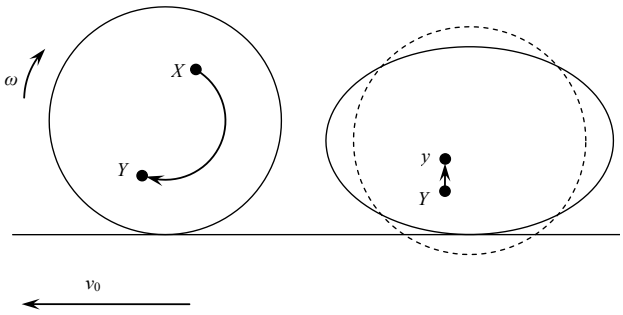

Fig. 2. Movement at the internal tire points

At point X, the final position at t is defined as

$$y = \chi\left(Y, t\right) \tag{2}$$

So the kinematic velocity of this point is

$$v = \dot{y} = \frac{\partial \chi}{\partial Y} \cdot \frac{\partial Y}{\partial t} + \frac{\partial \chi}{\partial t} \tag{3}$$

According to Eq. (1),

$$\frac{\partial Y}{\partial t} = \dot{R}_S \cdot X = \omega \mathrm{T} \times Y \tag{4}$$

The peripheral direction can be defined as:

$$\mathrm{S} = \frac{\mathrm{T} \times Y}{R} \tag{5}$$

where R is a rigid-rotating radius of point X.

According to Eqs. (4) and (5), Eq. (3) can be rewritten as

$$v = \omega R \frac{\partial \chi}{\partial Y} \cdot \mathrm{S} + \frac{\partial \chi}{\partial t} = \omega R \frac{\partial \chi}{\partial S} + \frac{\partial \chi}{\partial t} \tag{6}$$

where S is the arc length that point X makes a rigid rotation at t.

For steady-state conditions, $\partial\chi/\partial t = 0$, Eq. (6) can be simplified as

$$v = \omega R \frac{\partial \chi}{\partial S} \tag{7}$$

The time derivative of Eq. (7) is the accelerated velocity of point y:

$$a = \omega^2 R^2 \frac{\partial^2 \chi}{\partial S^2} \tag{8}$$

In the model, the virtual work contribution from D'Alembert forces is

$$\delta\Pi = -\int_V \rho a \cdot \delta v \mathrm{d}V = -\int_V \rho\omega^2 R^2 \frac{\partial^2 \chi}{\partial S^2} \cdot \delta v \mathrm{d}V \tag{9}$$

The virtual work contribution becomes

$$\frac{\partial}{\partial S}\left(\frac{\partial \chi}{\partial S}\cdot\delta v\right) = \frac{\partial^2 \chi}{\partial S^2}\cdot\delta v + \frac{\partial \chi}{\partial S}\cdot\frac{\partial \delta v}{\partial S} \tag{10}$$

Then, Eq. (9) can be rewritten as

$$\delta\Pi = -\int_V \rho\omega^2 R^2 \frac{\partial}{\partial S}\left(\frac{\partial \chi}{\partial S}\cdot\delta v\right)\mathrm{d}V + \int_V \rho\omega^2 R^2 \frac{\partial \chi}{\partial S}\cdot\frac{\partial \delta v}{\partial S}\mathrm{d}V \tag{11}$$

According to Eq. (3),

$$\frac{\partial}{\partial S} = \mathrm{S}\cdot\frac{\partial}{\partial Y} \tag{12}$$

Based on the divergence criterion, the first term in Eq. (11) can be expressed as

$$\int_V \rho\omega^2 R^2 \mathrm{S}\cdot\frac{\partial}{\partial Y}\left(\frac{\partial \chi}{\partial S}\cdot\delta v\right)\mathrm{d}V = \int_S \rho\omega^2 R^2 \mathrm{S}\cdot\mathrm{n}\left(\frac{\partial \chi}{\partial S}\cdot\delta v\right)\mathrm{d}S \tag{13}$$

where n is the unit vector along the normal direction of the curve.

As $\mathrm{S}\cdot\mathrm{n} = 0$, the virtual work contribution from D'Alembert forces becomes

$$\delta\Pi = \int_V \rho\omega^2 R^2 \frac{\partial \chi}{\partial S}\cdot\frac{\partial \delta v}{\partial S}\mathrm{d}V \tag{14}$$

The virtual work rate becomes

$$\mathrm{d}\delta\Pi = \int_V \rho\omega^2 R^2 \frac{\partial \mathrm{d}\chi}{\partial S}\cdot\frac{\partial \delta v}{\partial S}\mathrm{d}V \tag{15}$$

(2) Contact conditions

According to Eq. (6), the kinematic velocity of point y in relation to pavement is

$$v_r = v - v_0 = \omega R\frac{\partial \chi}{\partial S} + \frac{\partial \chi}{\partial t} - v_0 \tag{16}$$

Let h represent the distance between slave node and master control. The penetration rate is

$$\dot{h} = -\mathrm{n}\cdot v_r = v - v_0 = \mathrm{n}\cdot v_0 - \omega R\mathrm{n}\cdot\frac{\partial \chi}{\partial S} - \mathrm{n}\cdot\frac{\partial \chi}{\partial t} \tag{17}$$

For any contact point,

$$\mathrm{n}\cdot\frac{\partial \chi}{\partial S} = 0 \tag{18}$$

Therefore, Eq. (17) can be simplified as

$$\dot{h} = \mathrm{n}\cdot v_0 - \mathrm{n}\cdot\frac{\partial \chi}{\partial t} \tag{19}$$

Eq. (19) can be rewritten in the increment form, that is, the standard contact condition:

$$\Delta h = \mathrm{n}\cdot\left(\Delta x_0 - \Delta x\right) \tag{20}$$

For steady-state conditions, as $\mathrm{n}\cdot\Delta x_0 = \mathrm{n}\cdot\Delta x = 0$, $\Delta h = 0$.

The slip rate is defined as

$$\dot{\gamma} = \mathrm{t}_\alpha \cdot v_r = \omega R\mathrm{t}_\alpha \cdot\frac{\partial \chi}{\partial S} + \mathrm{t}_\alpha\cdot\frac{\partial \chi}{\partial t} - \mathrm{t}_\alpha\cdot v_0 \tag{21}$$

where t_α is the tangential vector of the contact surface, $\alpha = 1$, 2, and $\mathrm{n} = \mathrm{t}_1 \times \mathrm{t}_2$.

Under steady-state conditions, as $\partial\chi/\partial t = 0$, Eq. (21) is simplified as

$$\dot{\gamma} = \mathrm{t}_\alpha \cdot v_r = \omega R\mathrm{t}_\alpha \cdot\frac{\partial \chi}{\partial S} - \mathrm{t}_\alpha\cdot v_0 \tag{22}$$

The variation of $\dot{\gamma}$ is

$$\delta\dot{\gamma} = \mathrm{t}_\alpha \cdot v_r = \omega R\mathrm{t}_\alpha \cdot\frac{\partial \delta\chi}{\partial S} - \mathrm{t}_\alpha\cdot\delta v_0 \tag{23}$$

The Coulomb law of friction describes friction between contact surfaces. When the frictional force is smaller than the critical frictional force, the contact surfaces do not slip relatively. In this paper, the contact condition without a relative slip is expressed approximately as follows:

$$\tau_\alpha = \dot{\gamma}\frac{fp}{2F_f\omega R} \tag{24}$$

where τ_α ($\alpha = 1$, 2) is the tangential shear stress of contact surfaces, f is the friction coefficient, p is the contact pressure, and F_f is the allowable slip error.

The virtual work contribution from the slip is

$$\delta\Pi = \int_A \tau_\alpha \delta\gamma \, \mathrm{d}A \tag{25}$$

The virtual work rate for the slip is

$$\mathrm{d}\delta\Pi = \int_A \left(\mathrm{d}\tau_\alpha \delta\gamma + \tau_\alpha \mathrm{d}\delta\gamma\right)\mathrm{d}A \tag{26}$$

3.2 Tire model descriptions

To compare with the ESWL, the 11.00R20 tire is chosen for the tire force analysis. The section width, outer diameter, load capacity, and pressure of this tire are 293 mm, 1,085 mm, 30 kN, and 0.72 MPa, respectively. The tire model is composed of rubbers and reinforcements. Fig. 3 shows the meshes of each component.

The rubbers in different parts of the tire are simplified to the same material. The neo-Hookean model is selected to simulate its hyperelastic properties, and the Prony series formulation is employed to model its viscous properties. The reinforcements include radial ply and steel belts, which are regarded as linear-elastic materials. The reinforcements are modeled as surface membrane elements, which are embedded in the host continuum elements. The rim is regarded as a rigid body, and the bead is attached to it. The tire patterns are neglected, and tire heating is not considered. The pavement is simplified as a rigid surface in contact with the tire.

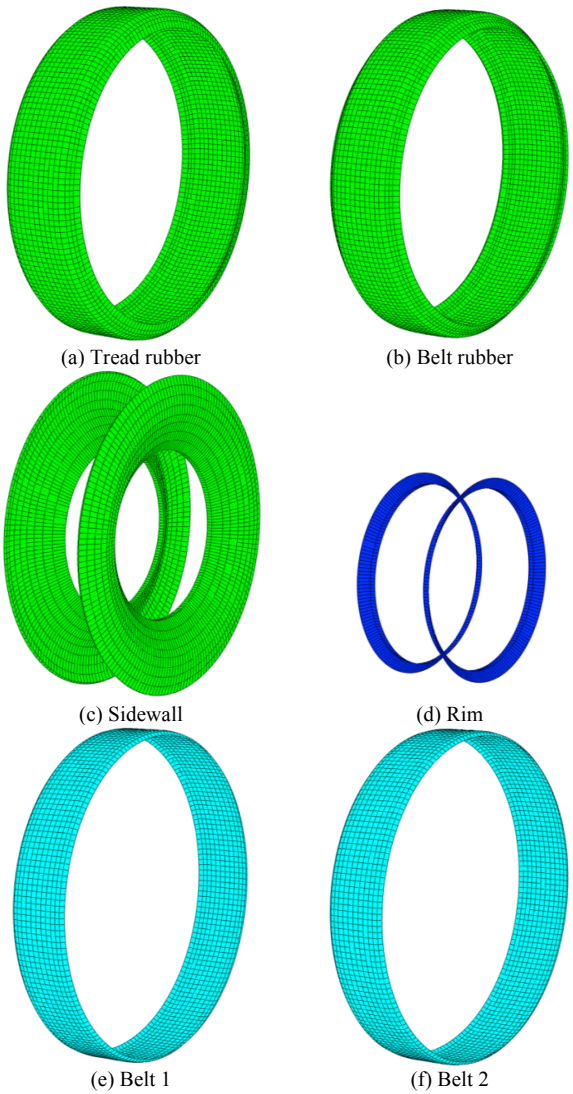

(a) Tread rubber (b) Belt rubber (c) Sidewall (d) Rim (e) Belt 1 (f) Belt 2

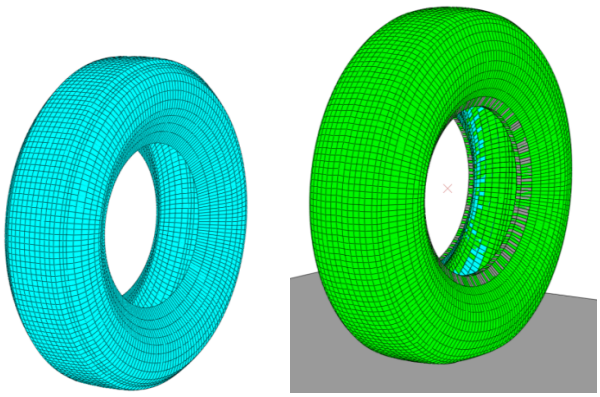

(g) Radial ply (h) Full tire

Fig. 3. 3D finite element model of the 11.00R20 tire

Tire rolling includes angular velocity ω and linear velocity v_0. The rotation axis of ω is parallel to the Y axis, and the v_0 direction is parallel to the X axis. The working condition of the vertical tire load is 25 kN, inflation tire pressure is 0.70 MPa, v_0 = 80 km/h, and f = 0.9. The pavement with no horizontal and vertical slopes is defined as the standard working condition. It is the common operation condition of truck tires on highways.

4. Result analysis and discussion

4.1 Tire-pavement contact stress under the standard working condition

According to simulation results, a complicated 3D contact stress exists between the tire and the pavement when the tire is under the steady-state rolling condition. The component forces of this contact stress along three directions of the coordinate system are recorded as CPRESS, CSHEAR1, and CSHEAR2, respectively. Tire contact stress under the free rolling state is shown in Fig. 4, and tire contact stresses under the complete braking and traction states are presented in Fig. 5.

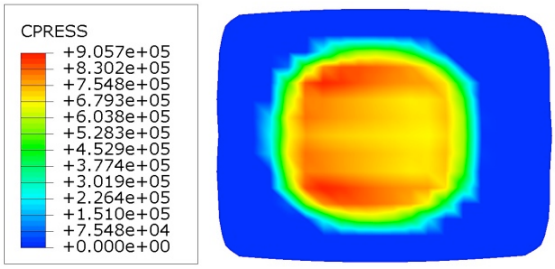

(a) Vertical stress

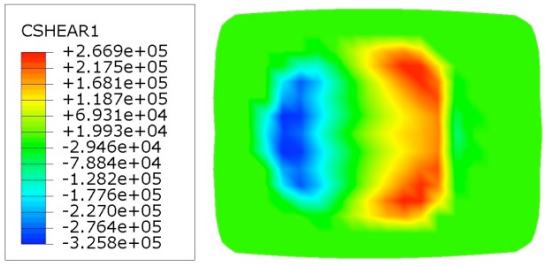

(b) Longitudinal stress

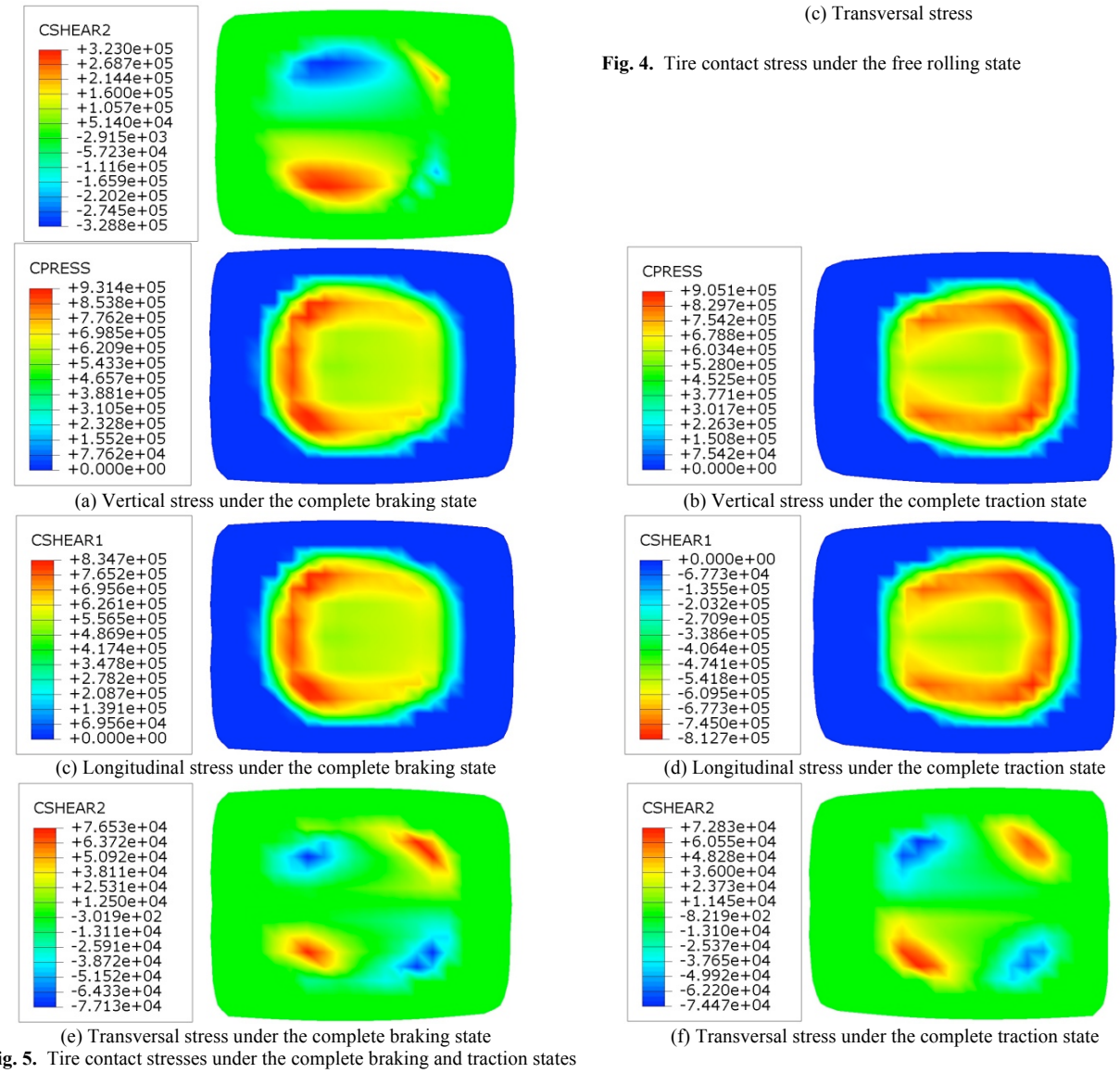

(a) Vertical stress under the complete braking state

(b) Vertical stress under the complete traction state

(c) Longitudinal stress under the complete braking state

(d) Longitudinal stress under the complete traction state

(e) Transversal stress under the complete braking state

(f) Transversal stress under the complete traction state

Fig. 5. Tire contact stresses under the complete braking and traction states

(c) Transversal stress

Fig. 4. Tire contact stress under the free rolling state

Figs. 4 and 5 show that when the tire is rolling, the predicted tire imprint is identical to that of the assumed ESWL, which is generally a circular shape. Tire imprint changes slightly with the rolling state change. However, the spatial distribution of the tire contact stress is far more complicated than the ESWL and shows different characteristics with the rolling state change.

Under free rolling, CPRESS distributes unevenly in the tire imprint, but such unevenness is not very distinctive. Therefore, assuming that CPRESS in ESWL is a uniform vertical load to some extent is reasonable. As the resultant force of CSHEAR1 and CSHEAR2 is close to 0, ESWL hypothesizes that the horizontal contact stress is 0. Nevertheless, the simulation results demonstrate that the extreme values of CSHEAR1 and CSHEAR2 are at the same magnitude of that of CPRESS, which differs significantly from the horizontal contact stress in ESWL. Therefore, compared with the predicted tire contact stress, ESWL greatly simplifies the horizontal tire force, which may make ESWL fail to predict accurately the mechanical behaviors and early damage of the pavement surface when it is used as the pavement design load.

Under the complete braking state, the CPRESS spatial distribution is the same as that under free rolling. It can still be simplified into a circular uniform load. The spatial distribution law of CSHEAR1 under the complete braking state is the same as that of CPRESS. The CSHEAR1 amplitude in the same position is the product of CPRESS and f. The CSHEAR2 amplitude is far smaller than that of CPRESS and CSHEAR1. Therefore, in pavement design, CPRESS and CSHEAR1 can be simplified into circular uniform loads under the complete braking state, and CSHEAR2 can be neglected.

The complete traction state can be viewed as the opposite of the complete braking state. Tire forces under these two states can be simplified into the same forms, except that CSHEAR1 under the complete traction state is opposite to that under the complete braking state.

4.2 Effects of tire operation parameters on contact stress

The effects of tire operation parameters (including axle load, tire pressure, v_0, and f) on contact stress are analyzed by changing the corresponding parameter of the standard working condition. As braking and traction are two completely opposite processes, the following discussion only analyzes the conditions under braking and free rolling.

(1) Axle load

According to the common truck design, the axle load range for a tire is 5-45 kN. The effect of axle load on contact stress is analyzed based on the standard working condition. Here, only the simulation of contact stress under 45 kN axle load is

presented (Fig. 6).

The simulation results indicate that axle load significantly influences contact stress. With the increase in axle load, tire footprint gradually changes from a circle to a rectangle. Tread CPRESS changes slightly, but the CPRESS of the tire shoulder increases. When the axle load exceeds 25 kN, tire shoulder stress is significantly higher than that on the tread. This finding reveals that overload is an important incentive in accelerating the wearing of the tire shoulder and accelerates the occurrence of early pavement failure.

(2) Tire pressure

Pressure of the 11.00R20 tire varies between 0.62 and 0.93 MPa. The tire pressure effect on tire contact stress is analyzed on the basis of the standard working condition. Here, only the tire contact stress simulation under 0.93 MPa tire pressure is presented (Fig. 7).

According to the simulation results, tire pressure greatly influences the tire contact stress. Under the same loading conditions, the contact area decreases with the increase in tire pressure, and the contact-stress distribution becomes increasingly uniform. This finding indicates that tire pressure can effectively improve the mechanical behaviors of tire under overloading conditions. However, a high tire pressure cannot significantly improve the mechanical behaviors of the pavement. Under overloading conditions, although a high tire pressure is conducive to a uniform spatial distribution of tire force, the axle load on the tire does not change. Conversely, contact stress on the tread tire is kept close to the tire pressure. Even under a low axle load, a high tire pressure may cause a relatively high contact stress.

(3) Pavement friction coefficient

The f changes with the changes in pavement temperature, humidity, and cleanliness. Under extreme conditions, such as snow cover or frozen pavement, f can reach as low as 0.3. The effect of f on the tire contact stress is analyzed on the basis of the standard working condition. Here, only the tire contact stress simulation when f = 0.3 is presented (Fig. 8).

According to the simulation results, CSHEAR1 is positively correlated with f, whereas tire imprint, CPRESS, and CSHEAR2 are independent from f. This finding demonstrates that low f may improve the mechanical behaviors of the pavement surface. However, such an improvement is at the cost of vehicular security because a low f reduces the adhesive force of the tire and weaken the braking performance of the tire.

(4) Linear velocity

Truck travel speed on a highway is generally 60-120 km/h. The effect of v_0 on the tire contact stress is analyzed on the basis of the standard working condition. The simulation indicates that under different travel speeds, the spatial distribution of contact stress changes slightly. The simulation of the tire contact stress when v_0 = 120 km/h is shown in Fig. 9.

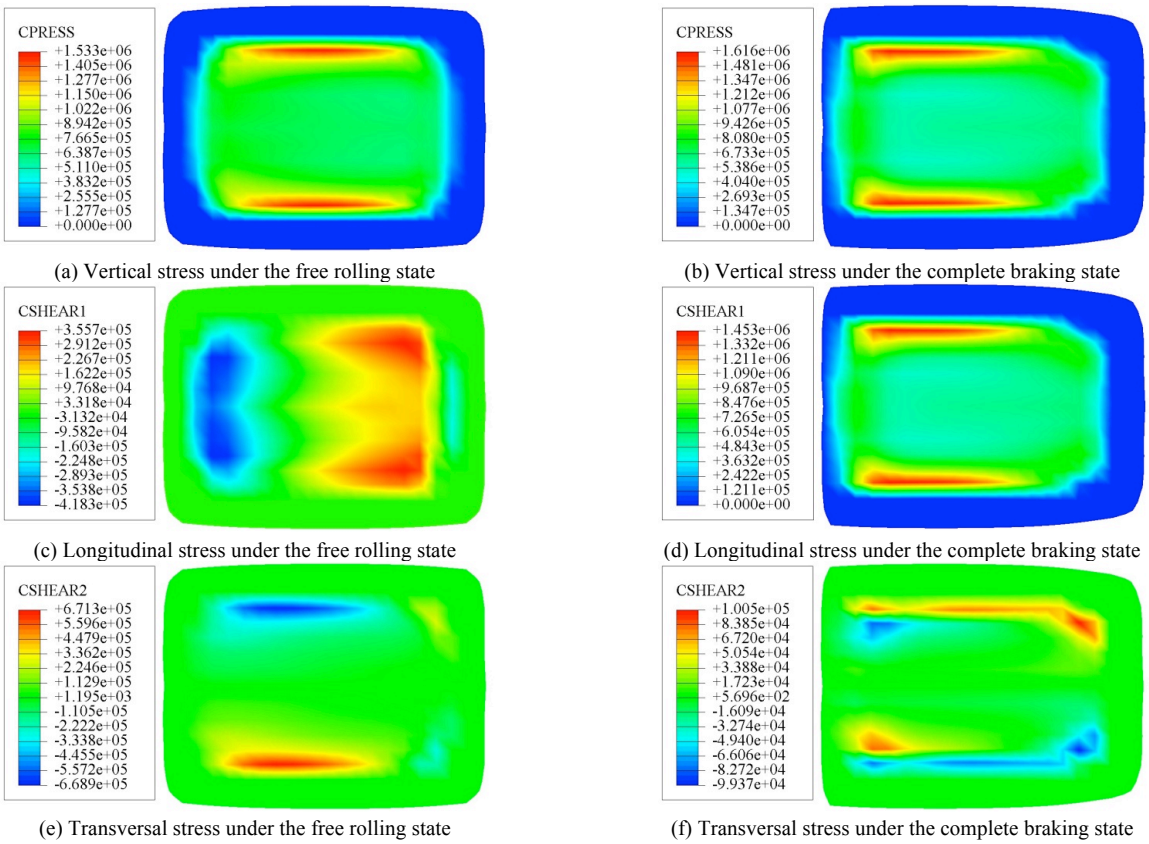

(a) Vertical stress under the free rolling state

(b) Vertical stress under the complete braking state

(c) Longitudinal stress under the free rolling state

(d) Longitudinal stress under the complete braking state

(e) Transversal stress under the free rolling state

(f) Transversal stress under the complete braking state

Fig. 6. Tire contact stress under a 45 kN axle load

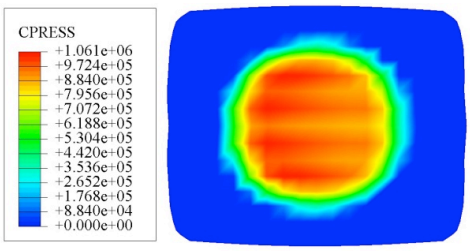

(a) Vertical stress under the free rolling state

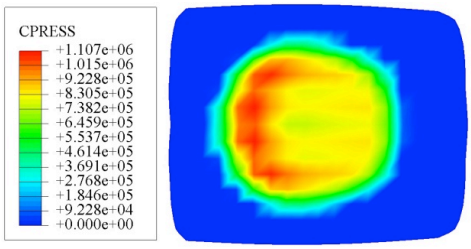

(b) Vertical stress under the complete braking state

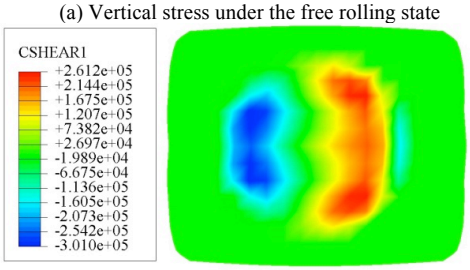

(c) Longitudinal stress under the free rolling state

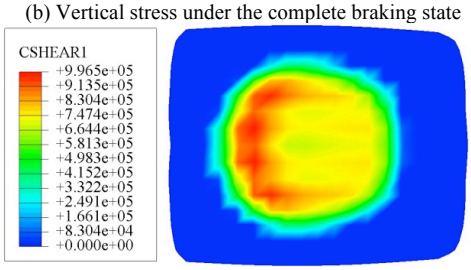

(d) Longitudinal stress under the complete braking state

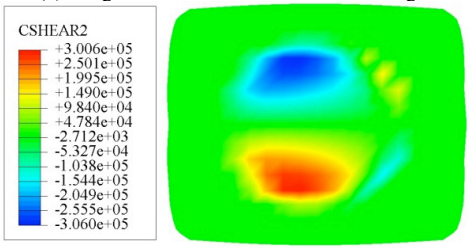

(e) Transversal stress under the free rolling state

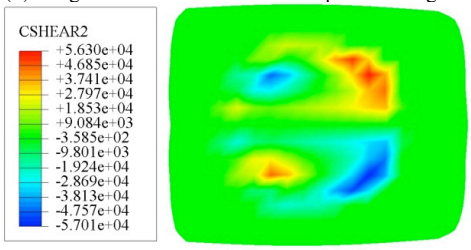

(f) Transversal stress under the complete braking state

Fig. 7. Tire contact pressure under 0.93 MPa tire pressure

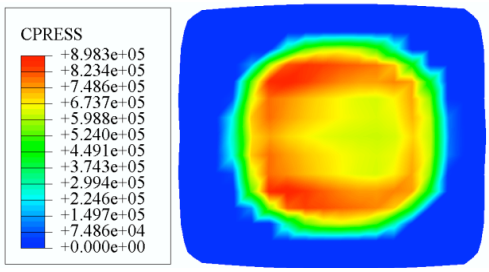

(a) Vertical stress under the free rolling state

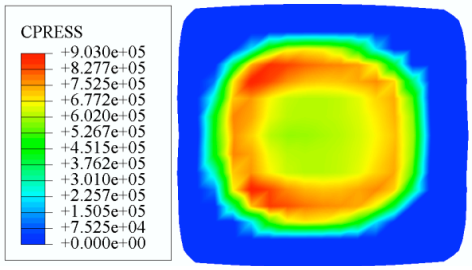

(b) Vertical stress under the complete braking state

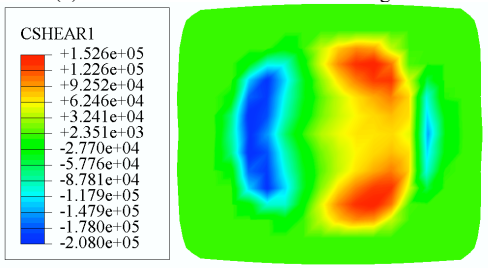

(c) Longitudinal stress under the free rolling state

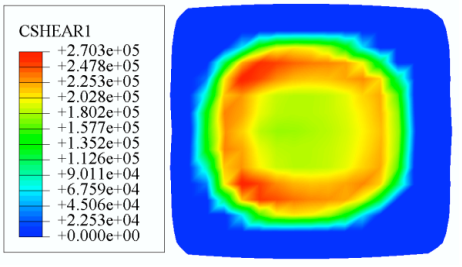

(d) Longitudinal stress under the complete braking state

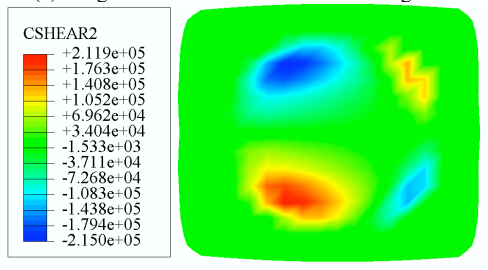

(e) Transversal stress under the free rolling state

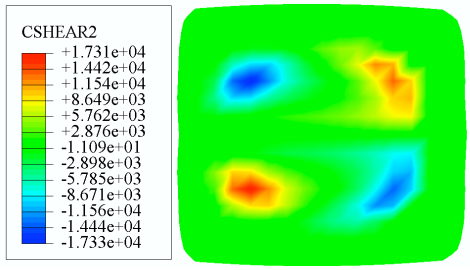

(f) Transversal stress under the complete braking state

Fig. 8. Tire contact stress when $f = 0.3$

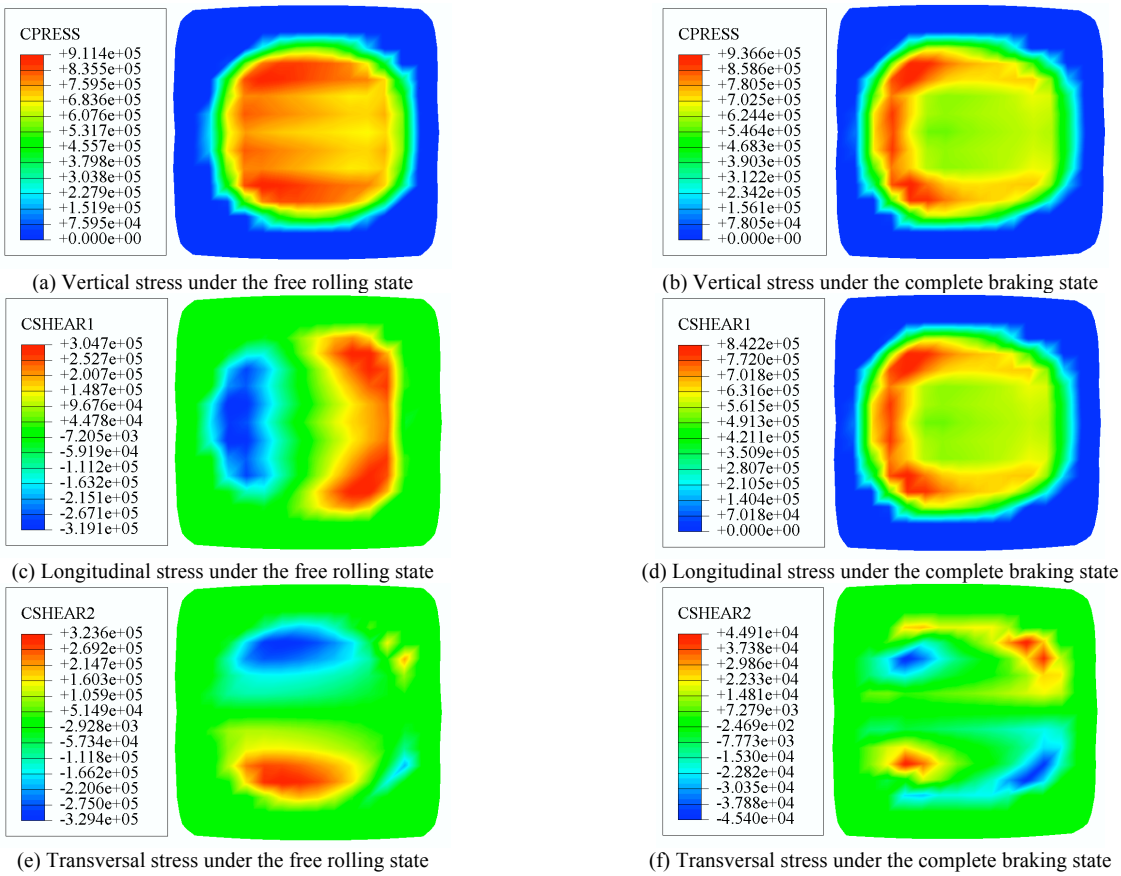

(a) Vertical stress under the free rolling state

(b) Vertical stress under the complete braking state

(c) Longitudinal stress under the free rolling state

(d) Longitudinal stress under the complete braking state

(e) Transversal stress under the free rolling state

(f) Transversal stress under the complete braking state

Fig. 9. Tire contact stress when v_0 =120 km/h

5. Conclusions

To predict the force of a typical truck tire on a highway, a finite element model of an 11.00R20 tire and a rigid surface is established on the basis of the mixed Eulerian/Lagrangian method. This model is used to predict tire contact stress under several working conditions. The following conclusions are obtained:

(1) Tire contact stress can be decomposed into the component force of three directions: CPRESS, CSHEAR1, and CSHEAR2. Under the steady-state rolling condition, these three component forces exist simultaneously, and CSHEAR1 and CSHEAR2 may have the same magnitude with CPRESS. However, CSHEAR1 and CSHEAR2 are considered 0 in the ESWL. Therefore, using ESWL as design load in the pavement model can make the model neither capable of predicting the mechanical behaviors of pavement structures accurately nor capable of simulating early failure mechanism of the pavement surface.

(2) Contact stress of the 11.00R20 tire for free rolling under the standard working condition is the most typical tire force form against a pavement. Under this condition, the tire footprint is approximately circular, and CPRESS can be viewed as a uniformly distributed force. The extreme values of CSHEAR1 and CSHEAR2 are at the same magnitude of CPRESS. CSHEAR1 and CSHEAR2 should not be neglected during mechanical pavement analysis.

(3) Given the standard working condition, CPRESS and CSHEAR1 can be considered uniformly distributed forces when the 11.00R20 tire is under complete braking or traction states, while CSHEAR2 can be neglected.

(4) Axle load is the most important influencing factor of tire contact stress. An overly high axle load causes an overly high contact stress on the tire shoulder. A higher tire pressure can improve the tire contact stress distribution effectively and is conducive to improve the working performance of an overloaded tire. CSHEAR1 is positively correlated with f. Although a low f is favorable to the improvement of the mechanical behaviors of pavement structures, f should be kept at a high level for the sake of travel security. Moreover, travel speed effects on the tire contact stress can be neglected.

The predicted spatial distribution pattern of the tire contact stress can be used as reference for tire load modeling in a pavement model. Further studies can predict the contact stress of arabesquitic tires based on the established model to provide support for a more refined pavement model.

Acknowledgements

This study was supported by the National Natural Science Foundation of China for the financial support (Grant Nos. 11302138, 11172183, and 11102121).

References

1. Kim, M., Lee, J. H., "Study on nonlinear pavement responses of low volume roadways subject to multiple wheel loads". *Journal of Civil Engineering and Management*, 17(1), 2011, pp. 45-54..

2. Liu, Q., Shalaby, A., "Simulation of pavement response to tire pressure and shape of contact area". *Canadian Journal of Civil Engineering*, 40(3), 2013, pp. 236-242.

3. Khavassefat, P., Jelagin, D., Birgisson, B., "Dynamic response of flexible pavements at vehicle-road interaction". *Road Materials and Pavement Design*, 16(2), 2015, pp. 256-276.
4. Li, L., He, Z., Jiang, J., Lei, T., "Calculation method and influence law of pavement rut under dynamic load". *Journal of Testing and Evaluation*, 44(2), 2016, pp. 827-837.
5. De Beer, M., Maina, J. W., van Rensburg, Y., Greben, J. M., "Toward using tire-road contact stresses in pavement design and analysis". *Tire Science and Technology*, 40(4), 2012, pp. 246-271.
6. Wang, G., Roque, R., "Three-dimensional finite element modeling of static tire-pavement interaction". *Transportation Research Record: Journal of the Transportation Research Board*, (2155), 2010, pp. 158-169.
7. Moslem, N., Hossein, G., "Numerical simulation of tire/soil interaction using a verified 3D finite element model". *Journal of Central South University*, 21(2), 2014, pp. 817-821.
8. Xia, K., "Finite element modeling of tire/terrain interaction: Application to predicting soil compaction and tire mobility". *Journal of Terramechanics*, 48(2), 2011, pp. 113-123.
9. Xia, K., Yang, Y., "Three-dimensional finite element modeling of tire/ground interaction". *International Journal for Numerical and Analytical Methods in Geomechanics*, 36(4), 2012, pp. 498-516.
10. Li, H., Schindler, C., "Three-dimensional finite element and analytical modelling of tyre–soil interaction". *Journal of Multi-body Dynamics*, 227(1), 2013, pp. 42-60.
11. Li, H., Schindler, C., "Investigation of tire-soil interaction with analytical and finite element method". *Mechanics Based Design of Structures and Machines: An International Journal*, 41(3), 2013, pp. 293-315.
12. Wang, Y., Lu, Y. J., Si, C. D. Sung, P., "Tire-pavement coupling dynamic simulation under tire high-speed-rolling condition". *International Journal of Simulation Modelling*, 15(2), 2016, pp. 236-248.
13. Al-Qadi, I. L., Wang, H., "Prediction of tire pavement contact stresses and analysis of asphalt pavement responses: A decoupled approach". *Journal of the Association of Asphalt Paving Technologists*, 80, 2011, pp. 289-316.
14. Wang, H., Ozer, H., Al-Qadi, I. L., Duarte, C. A., "Analysis of near-surface cracking under critical loading conditions using uncracked and cracked pavement models". *Journal of Transportation Engineering*, 139(10), 2013, pp. 992-1000.
15. Dong, Z., Tan, Y., Ou, J., "Dynamic response analysis of asphalt pavement under three-directional nonuniform moving load". *China Civil Engineering Journal*, 46(6), 2013, pp. 122-130.
16. Hu, X., Walubita, L. F., "Modeling mechanistic responses in asphalt pavements under three-dimensional tire-pavement contact pressure". *Journal of Central South University of Technology*, 18(1), 2011, pp. 250-258.
17. Bonse, R. P., Kuhn, S. H., "Dynamic forces exerted by moving vehicles on a road surface". *Highway Research Board Bulletin*, (233), 1959, pp. 9-32.
18. Seitz, N., Hussmann, A., "Forces and displacement in contact area of free rolling tires". *SAE Technical Paper 710626*, 1971.
19. Lippmann, S. A., Oblizajek, K. L., "The distributions of stress between the tread and the road for freely rolling tires". *SAE Technical Paper 740072*, 1974.
20. Howell, W. E., Perez, S. E., Vogler, W. A., "Aircraft tire footprint forces". In: *The Tire Pavement Interface,* Philadelphia, USA: ASTM, 1986, pp. 110-124.
21. Zhang, Y., Yi, J., Liu T., "Embedded flexible force sensor for in-situ tire–road interaction measurements". *IEEE Sensors Journal*, 13(5), 2013, pp. 1756-1765.
22. Hernandez, J., Al-Qadi, I., De Beer, M., "Impact of tire loading and tire pressure on measured 3D contact stresses". In: *Airfield and Highway Pavement 2013: Sustainable and Efficient Pavements - Proceedings of the 2013 Airfield and Highway Pavement Conference*, Los Angeles, USA: ASCE, 2013, pp. 551-560.
23. Luo, R., Prozzi, J. A., "Effect of measured three-dimensional tire-pavement contact stress on pavement response at asphalt surface". *Transportation Research Record: Journal of the Transportation Research Board*, (2037), 2007, pp. 115-127.
24. Yang, J., Ong, G. P., Fwa, T. F., Chew, C. H., "Modeling the effect of rolling conditions on stress development at tire-pavement contact patch". *Asian Transport Studies*, 2(2), 2012, pp. 139-152.
25. Wang, H., Al-Qadi, I. L., Stanciulescu, I., "Effect of surface friction on tire-pavement contact stresses during vehicle maneuvering". *Journal of Engineering Mechanics*, 140(4), 2014, Paper No. 04014001.
26. Hernandez, J., Al-Qadi, I. L., "Hyperelastic modeling of wide-base tire and prediction of its contact stresses". *Journal of Engineering Mechanics*, 142(2), 2015, Paper No. 04015084.